$^{40}Ar/^{39}Ar$ age of the Rotoiti Breccia and Rotoehu Ash, Okataina Volcanic Complex, New Zealand, and identification of heterogeneously distributed excess ^{40}Ar in supercooled crystals.

Stephanie Flude[a1] and Michael Storey[a]

[a]Quaternary Dating Laboratory, Department of Environmental, Social and Spatial Change, Roskilde University, DK-4000 Roskilde, Denmark.

[1]Corresponding author. Present address: School of Geosciences, The University of Edinburgh, The Grant Institute, The Kings Buildings, Edinburgh EH9 3JW, United Kingdom. Email: sflude@gmail.com; tel: +44 (0)131-650-7010; fax: +44(0)131- 650-7340

Abstract

Co-magmatic granitoid clasts erupted as part of the Rotoiti Ignimbrite (Rotoehu Tephra) contain euhedral K-feldspar and biotite crystals that protrude into miarolytic cavities and show textural evidence for growth in super-cooled conditions, thus are interpreted as growing during eruption. $^{40}Ar/^{39}Ar$ stepped heating experiments on single K-feldspar crystals reveal the presence of heterogeneously distributed excess ^{40}Ar, preferentially released at lower temperature steps (most likely from fluid/melt inclusions), which cannot reliably be characterised by, or corrected for using isotope correlation diagrams due to mixing between three reservoirs of ^{40}Ar (radiogenic, atmospheric and excess). This excess ^{40}Ar component is common, but not ubiquitous, and an age population unmixing algorithm applied to single-crystal fusion data identifies a younger group of K-feldspar and biotite crystals that appear to be largely unaffected by excess ^{40}Ar. This population gives a statistically robust weighted mean age of 47.4 ± 1.5 ka (1σ, n = 13) and an indistinguishable inverse isochron age of 50 ± 3 ka for this historically difficult to date eruption. The weighted mean age is significantly younger than previous age estimates of the Rotoiti eruption obtained by K/Ar and $^{40}Ar/^{39}Ar$ dating of bracketing lavas, but is indistinguishable from recent ^{14}C and (U-Th)/He dates and estimates based on orbital tuning and sedimentation rates constrained by ^{14}C ages.

Keywords

Rotoiti ignimbrite eruption; $^{40}Ar/^{39}Ar$; excess-^{40}Ar; Taupo Volcanic Zone

1. Introduction

The Rotoiti ignimbrite and Rotoehu ash, erupted from the Okataina Caldera in the Taupo Volcanic Zone (TVZ) and immediately followed by the eruption of the Earthquake Flat (EQF) ignimbrite, is an important regional stratigraphic marker on the North Island of New Zealand and in the SW Pacific Ocean which has been used to correlate numerous stratigraphic sections both onshore and offshore (e.g. Berryman, 1992; Molloy et al., 2008; Nilsson et al., 2011; Shane et al., 2006). It occurs at the base of a remarkably well constrained tephra record in which all deposits have been correlated to their source vents and their distribution is well known (Shane, 2000) and so an accurate age for this deposit is particularly important for calculating both sedimentation rates and magma production and eruption rates in the TVZ and surrounding areas. Furthermore, the climatic conditions before and after the eruption are well constrained and the ash is interpreted to have been deposited during an interstadial, most likely in the middle of Marine Isotope Stage (MIS) 3 (Mcglone et al., 1984; Shane and Sandiford, 2003). However, despite 45 years of study and numerous attempts to date the eruption, the age of the Rotoehu ash still remains controversial, with recent published ages ranging from ~45 to 61 ka. In this paper we present $^{40}Ar/^{39}Ar$ stepped heating and total fusion data for single crystals of K-feldspar and biotite from co-magmatic granitoid lithic clasts erupted as part of the Rotoiti ignimbrite and show that the eruption most likely took place at ~ 47 ka.

1.1 Geological context

The 60 km wide Taupo Volcanic Zone (TVZ) extends ~300 km north-eastwards from the centre of the North Island of New Zealand into the Bay of Plenty and the south Pacific Ocean (Figure 1). Volcanism in the TVZ began at ~2 Ma, becoming dominated by silicic volcanism after ~1.6 Ma and it is currently the most active region of silicic volcanism on Earth, with rhyolite eruption rates of 3.8 $km^3\ ka^{-1}$ (over the last 1.6 Ma). There are at least 8 caldera complexes that have been active over the lifetime of the TVZ, with at least 34 caldera forming eruptions identified as having occurred since 1.6 Ma (Wilson et al., 1995). The Okataina caldera complex (also referred to as the Haroharo Caldera complex, Charlier et al., 2003; Shane et al., 2012; Smith et al., 2010) is one of the most productive silicic volcanoes known with rhyolite production rates quoted as being 2.5 $km^3\ ka^{-1}$ over the last 65 ka (Wilson et al., 1995). The Rotoiti ignimbrite (also referred to as the

57 Rotoiti breccia) and Rotoehu ash were produced during the most recent caldera collapse eruption of the
58 Okataina caldera. The eruption began with an explosive basaltic eruption, producing the Matahina Tephra
59 (Pullar and Nairn, 1972) and was immediately followed by the Rotoiti eruption which produced non-welded
60 ignimbrite, interbedded with and overlain by phreatomagmatic ash, with the combined ignimbrite and ash
61 equating to a magma volume of at least 80 km^3 (Wilson et al, 2007). The Rotoiti eruption was followed
62 almost immediately (within months) by the smaller volume (7 km^3 of magma) Earthquake Flat ignimbrite
63 and associated Rifle Range ash (Nairn and Kohn, 1973; Wilson et al., 2007), which is generally considered to
64 originate from the Kapenga caldera complex, although Burt et al. (1998) suggested that the EQF vent
65 lineament represents a cryptic ring-shaped structural boundary of the Okataina volcanic centre (Figure 1B).

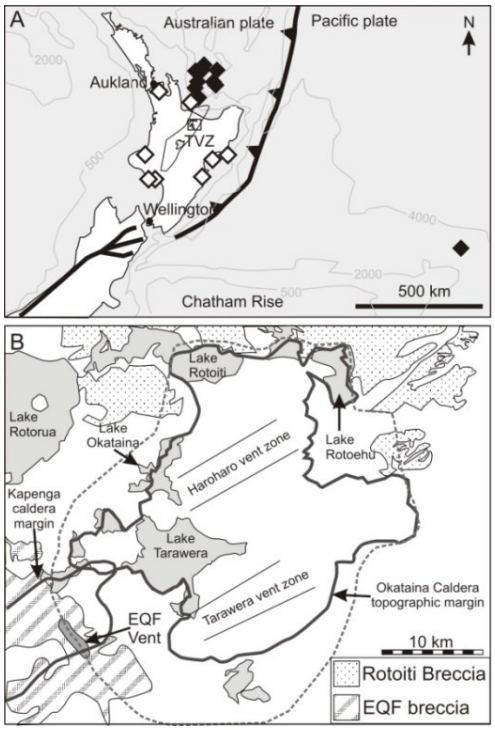

Fig. 1. (A) – Map showing the tectonic setting of the Taupo Volcanic Zone (TVZ), related to the subduction of the Pacific plate beneath the Australian plate, with onshore (white diamonds) and offshore (black diamonds) occurrences of the Rotoiti Ignimbrite and / or Rotoehu ash (Allan et al., 2008; Berryman, 1992; Danišík et al., 2012; Molloy et al., 2009; Nairn and Kohn, 1973; Santos et al., 2001; Shane et al., 2006; Shane and Sandiford, 2003). Square box shows the location of Figure. 1B. (B) – Structural map of the Okataina Caldera, the source of the Rotoiti eruption (after Charlier and Wilson, 2010). Dashed line represents the cryptic structural boundary of the Okataina caldera as suggested by Burt et al. (1998).

65 Plutonic lithic fragments brought to the surface during ignimbrite eruptions have been observed in many
66 TVZ volcanic deposits (Brown et al., 1998; Burt et al., 1998; Charlier et al., 2003; Ewart and Cole, 1967;
67 Shane et al., 2012). However, a notable class of felsic plutonic clasts contained in a lithic lag breccia facies
68 of the Rotoiti ignimbrite contain volcanic glass, indicating that they were incompletely crystallised at depth
69 and so are referred to as granitoids (Brown et al., 1998; Burt et al., 1998). The most common type of these

granitoid clasts, Group 1 granitoids (the subject of this study), tend to be highly friable, exhibit quench textures, such as volcanic glass, micrographic intergrowths and miarolytic cavities lined with euhedral crystals, and often contain two populations of biotite (Brown et al., 1998; Burt et al., 1998; Charlier et al., 2003). Importantly, the glass in these granitoid fragments often co-exists with euhedral crystals, implying that the glass represents quenched residual melt, rather than melt infiltration and remobilisation of a previously solidified magma body, which would result in rounded and resorbed crystals (Brown et al., 1998; Burt et al., 1998). Based on contrasting chemical and isotopic signatures, the granitoid clasts are generally considered to be co-magmatic, rather than cognate or xenolithic, to the Rotoiti ignimbrite magma, forming from a spatially close but petrogenetically distinct magma batch (possibly derived from the Matahina magmatic system) that was emplaced at a high crustal level and subsequently disturbed during the caldera-collapse phase of the Rotoiti eruption (Brown et al., 1998; Burt et al., 1998; Charlier et al., 2003; Shane et al., 2005). Cooling and crystallisation of the Group 1 granitoids is generally considered to have taken place in at least two stages, with most crystallisation taking place at 10-15 km depth, followed by volatile-loss, undercooling and crystallisation at < 3 km, associated with upheaval caused by migration of the Rotoiti magma towards the surface (Brown et al., 1998; Burt et al., 1998).

1.2 Previous age estimates for the Rotoiti eruption

The range of published ages for the Rotoiti eruption is given in Table 1, along with pertinent details, and in Figure 2 (all ages in this paper are quoted as ± 1σ, where known). The earliest attempts to assign an age to the Rotoiti eruption utilised radiocarbon dating and were plagued by difficulties relating to the age limit for ^{14}C dating (generally considered to be ~40-50 ka) and contamination with younger carbon material (Froggatt and Lowe, 1990; Grant-Taylor and Rafter, 1971; Lowe and Hogg, 1995; Nairn and Kohn, 1973; Nathan, 1976; Pillans and Wright, 1992; Pullar, 1976; Pullar and Heine, 1971; Shane, 2000; Thompson, 1968a; Vucetich and Pullar, 1969; Whitehead and Ditchburn, 1994). For many years, Wilson et al.'s (1992)

Method	Unit	Age (ka) ±1σ	Notes	References
^{14}C (pre-2000)	Rotoiti breccia and ash	31 - > 41	Ages at limit of detection and contaminated by younger carbon.	1-8, 10, 12, 17, 18
^{238}U-^{230}Th disequilibrium	Rotoehu ash	71 ± 6	Data considered invalid by refs 10,18	9
Electron spin resonance	Rotoiti breccia	45.2 ± 8.2	Refs 9 and 10 suggest data may be invalid due to U-Th disequilibrium.	11
Marine sedimentation rates	Rotoehu ash	~55	Tephra not conclusively identified	12
K/Ar	Mayor island lava bracketing Rotoehu ash	64 ± 4	Overlying lava = 67 ±11 ka. Underlying lava = 63 ± 5 ka	13
Stratigraphic age	Extrapolation between marine terrace ages formed pre and post deposition	52 ± 7	Ages of bracketing terraces = 40 and 59 ka. Ages of terraces refined to ~43 and 61 ka respectively by ref 21.	14,15
Amino acid racemization	Palaeosols bracketing Rotoiti breccia and ash	~61		16
Optical Luminescence Dating	Underlying and overlying palaeosols from 2 sections	42 ± 8 - 34 ± 3 44 ± 3 - 30 ± 2		19
^{14}C-AMS	Wood below the Rotoehu ash	43.2± 0.6		20
^{238}U-^{230}Th disequilibrium	Rotoehu ignimbrite – xenolith: Rotoehu ignimbrite - pumice	57 ± 8 $> 29 \pm^{21}_{17}$	Whole rock – magnetite – biotite Zircons	22
Lake sedimentation rates	Rotoehu ash	44.3	Palynology suggests Rotoehu ash deposited during MIS 3, i.e. between 59.1 and 29.0 ka	23
Lake sedimentation rates	Rotoehu ash	48.9	Composite depth scale calibrated by overlying ^{14}C dating of tephra	24
Marine sedimentation rates	Rotoehu ash	~45	Multiple deep sea sediment cores with chronology based on ^{14}C and Th/U-^{14}C ages of coral and foraminifera.	25
Combined K-Ar and ^{40}Ar/^{39}Ar	Mayor island lava bracketing Rotoehu ash	61.0 ± 1.4	Ar/Ar dates from crystals from Rotoiti and EQF eruptions give ages of 47 - 125 ka	26
Orbitally tuned marine sediment	Rotoehu ash	45.1		27
Lake sedimentation rates	Rotoehu ash	46-52	Sedimentation rates extrapolated from the between overlying Maketu and Tahuna tephra layers	28
^{14}C-AMS	Underlying / Overlying Rotoehu ash	47.5 ± 2.1 44.8 ± 0.3	Ages calibrated to calendar years BP	29
(U-Th)/He	Rotoiti Breccia / Earthquake Flat Pumice	45.1 ± 3.3 45.1 ± 2.9		29

Table 1. Published age estimates of the Rotoiti eruption, in order of publication. 1 (Thompson, 1968b), 2 (Vucetich and Pullar, 1969), 3 (Pullar and Heine, 1971), 4 (Grant-Taylor and Rafter, 1971), 1971, 5 (Nairn and Kohn, 1973), 6 (Nathan, 1976), 7 (Pullar, 1976), 8 (Mcglone et al., 1984), 9 (Ota et al., 1989), 10 (Froggatt and Lowe, 1990), 11 (Buhay et al., 1992), 12 (Pillans and Wright, 1992), 13 (Wilson et al., 1992), 14 (Berryman, 1992), 15 (Berryman, 1993), 16 (Kimber et al., 1994), 17 (Whitehead and Ditchburn, 1994), 18 (Lowe and Hogg, 1995), 19 (Lian and Shane, 2000), 20 (Santos et al., 2001), 21 (Chappell, 2002), 22 (Charlier et al., 2003), 23 (Shane and Sandiford, 2003), 24 (Nilsson et al., 2011), 25 (Shane et al., 2006), 26 (Wilson et al., 2007), 27 (Allan et al., 2008), 28 (Molloy et al., 2008), 29 (Danišík et al., 2012)

age of 64 ± 4 ka, based on K/Ar dating of overlying (67 ± 11 ka) and underlying (63 ±5 ka) obsidian lava flows on Mayor Island was considered to be the most reliable age for the Rotoiti eruption. This age was subsequently revised to 61.0 ± 1.4 ka based on a $^{40}Ar/^{39}Ar$ stepped heating plateau age of 58.5 ± 1.1 ka for the overlying Mayor Island obsidian lava flow and supported by stepped heating experiments on biotite and plagioclase from the Rotoiti and EQF ignimbrites, which showed a high level of xenocrystic contamination (Wilson et al., 2007). Indeed, ^{238}U-^{230}Th disequilibrium dating of both Rotoiti pumice and granitoid clasts and of the EQF ignimbrite indicates a prolonged crystallisation history, with isochron and weighted mean ages ranging from 51 ± 14.5 ka to 122^{+9}_{-8} ka (Charlier et al., 2003; Charlier and Wilson, 2010; Danišík et al., 2012). Danišík et al. (2012) addressed the problem of age-inheritance in zircons by carrying out (U-Th)/He dating, a method that has the advantage of avoiding potential pre-eruptive inheritance issues because of the high diffusion rate of ^{4}He at magmatic temperatures. They produced indistinguishable ages of 45.1 ± 3.3 and 45.1 ± 2.9 ka for the Rotoiti and EQF eruptions respectively. They also, along with Santos et al. (2001) addressed earlier problems with ^{14}C dating of the Rotoiti eruption by utilising high-sensitivity Accelerator Mass Spectroscopy (AMS) and improved sample preparation procedures to remove contaminating younger carbon, producing ^{14}C ages for material underlying and overlying the Rotoehu ash that are consistent with the (U-Th)/He dates. This younger date is also consistent with numerous age estimates (generally 45-50 ka) based on marine and lake sedimentation rates, calibrated by ^{14}C dating of younger tephras (Allan et al., 2008; Molloy et al., 2009; Nilsson et al., 2011; Pillans and Wright, 1992; Shane et al., 2006; Shane and Sandiford, 2003) and with Optical Luminescence (OSL) dating of palaeosols above and below the Rotoiti deposits. A slightly older (but with larger errors, overlapping most other age estimates) stratigraphic age for the Rotoehu ash of 52 ± 7 ka was proposed by Berryman, (1992, 1993) based on correlation of sediments bound by ages of marine terraces. The bounding terrace ages (40 ka and 59 ka) were based on correlation with marine terraces at the Huon Peninsula, New Guinea, dated by ^{14}C and $^{230}Th/^{234}U$ dating of corals (Chappell and Shackleton, 1986). Wilson et al. (2007) noted an updated age for the terraces (Chappell, 2002) and suggested that, according to Berryman's correlations, the Rotoiti eruption must have occurred between 72.8 ± 1.1 and 51.8 ± 0.4 ka. However, these ages are based on incorrect identification of the relevant marine terraces, probably due to inconsistencies in terrace naming

between Chappell and Shackleton (1986) and Chappell (2002); the correct age for the older terrace is 61.4 ka and the younger terrace was not re-dated, but is likely ~43 ka, based on extrapolation between older (43.9 ka) and younger (42.1 ka) terraces, suggesting that the Rotoiti eruption took place between 61.4 and 43 ka.

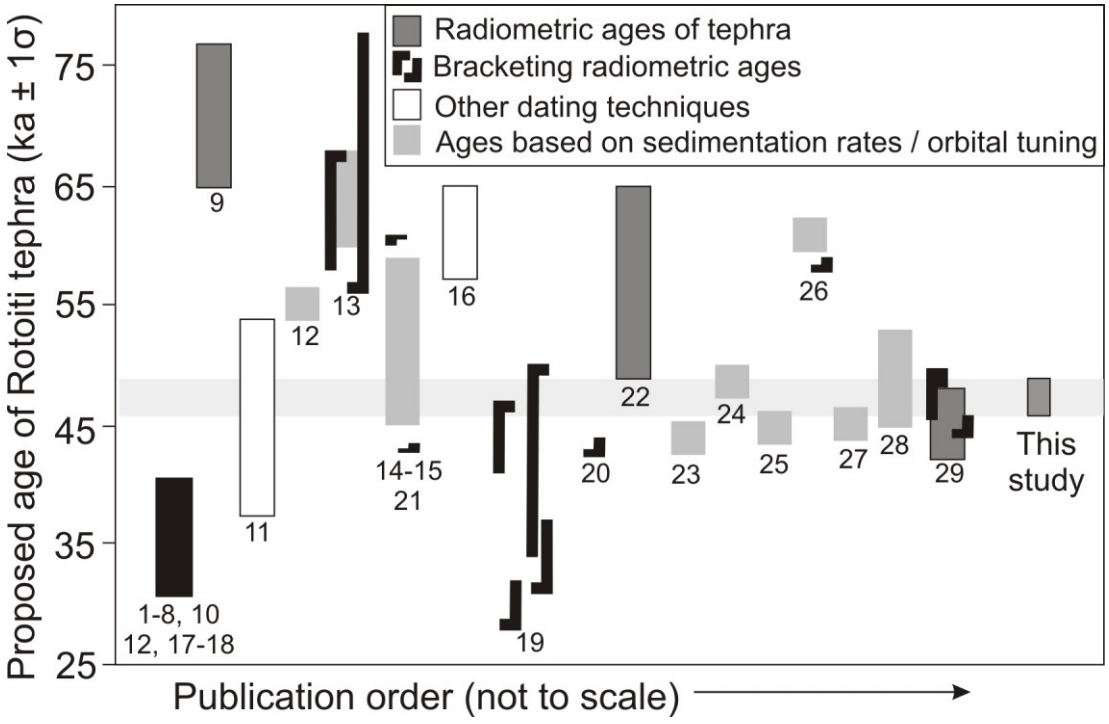

Figure 2. Schematic diagram showing ages published for the Rotoiti eruption. Vertical bars represent 1 standard deviation of published ages, or set as arbitrary squares where errors are not available (12, 16, 23-25, 27). Numbers refer to the references cited in Table 1. The horizontal grey bar represents the age ± 1 σ determined in this study.

2. Samples and methodology

Despite evidence of pre-eruption age zircons and thus an extended crystallisation history of Group 1 granitoid fragments (Charlier et al., 2003), the abundant quench textures which they exhibit indicate that at least part of the clasts crystallised during eruption. Sample 103/1, collected from the same granitoid block as sample 103/2, analysed by Charlier et al. (2003), contains abundant glass and miarolytic cavities lined with euhedral K-feldspar, quartz and biotite, which we interpret as having crystallised and quenched during eruption.

A polished thin section was prepared by impregnating a split of the sample with blue epoxy to highlight the miarolytic cavities and porosity of the sample. This section (Figure 3) exhibits many of the quench features identified by Burt et al. (1998) and Charlier et al. (2003), such as granophyric texture, along with euhedral quartz and K-feldspar crystals forming linings to the miarolytic cavities. Optical petrography of the euhedral K-feldspars shows that they are highly strained, exhibiting strongly developed cleavage planes, patchy, streaky and undulose extinction and, in some crystals, kinked cleavage planes and fine-scale structures in the core of the crystal, that appear streaky under both PPL and XPL (Figure 3B). These structures are similar in appearance to plagioclase-alkali feldspar intergrowths, and patchy extinction and sector zoning formed during sanidine crystallisation from an undercooled melt (Lofgren and Gooley, 1977). We interpret these feldspar textures as representing a combination of crystallisation during melt undercooling, and deformation during shearing processes during mobilisation and eruption, a process considered to be ubiquitous in the Group 1 granitoids (Brown et al., 1998; Burt et al., 1998).

Element mapping and semi-quantitative spot analyses were carried out on the polished section using a Bruker-nano M4 Tornado benchtop micro-XRF system. Analysis conditions, a summary of the technique and all semi-quantitative data are given in the supplementary information and Supplementary Data Table S1. A major element map displaying Si, K and Fe is shown in Figure 3A. The large area (1.5 ×2.5 cm) covered by the x-ray map reveals that many of the granophyric intergrowths radiate towards the miarolytic cavities, often terminating with euhedral quartz and K-feldspar crystals that project into the cavity.

A semi-quantitative chemical composition profile across a euhedral K-feldspar crystal (Figure 3D) suggests cryptic normal zoning, with relative Na-enrichment in the core and K-enrichment at the rim. Spot analyses of the fine-scale structures in Figure 3b indicate a relative enrichment of CaO and Na_2O and depletion of K_2O, consistent with our interpretation that they represent plagioclase – K-feldspar intergrowths during undercooling.

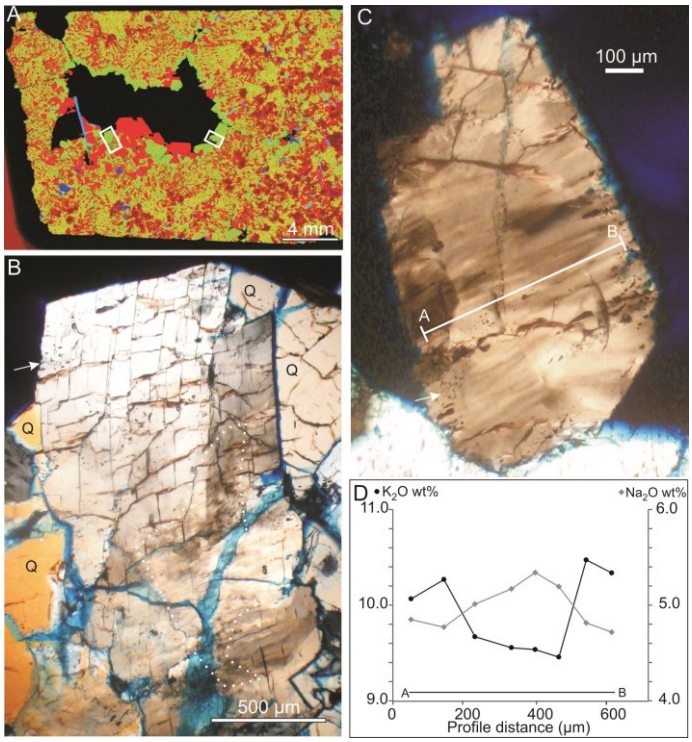

Figure 3. A) µ-XRF element map from a polished section of a miarolytic cavity in a granitoid clast. Elements are displayed as Si = red, K = green and Fe = blue, therefore quartz displays as bright red, K-feldspar as green, plagioclase as dark red and biotite and Fe-oxides as blue. White boxes show the positions of panels B (left) and C (right). B) XPL photomicrograph of an alkali feldspar crystal protruding into the miarolytic cavity. The white dotted line highlights fine-scale textures interpreted as plagioclase – K-feldspar intergrowths. Q = quartz crystals. C) XPL photomicrograph of an alkali feldspar crystal that grew into the miarolytic cavity. The crystal displays streaky and patchy extinction. The line a-b shows the position of the semi-quantitative chemical profile shown in panel (D) (see supplementary information for details). In the photomicrographs, white arrows highlight regions in the crystals rich in fluid and / or magmatic inclusions. Blue colouration is from impregnation during section preparation and highlights the permeable nature of the granitoids.

0.5-1 mm euhedral K-feldspar and 1-2 mm biotite crystals were hand-picked from miarolytic cavity linings of the kind illustrated in Figure 3A and prepared for irradiation for Ar-isotope analysis using standard techniques (see supplementary information). Given the likely extended crystallisation history of the granitoid clasts, all Ar-isotope analyses were carried out on single crystals to enable identification of any crystals that record pre-eruptive ages and prevent mixing of crystal populations. We carried out a

combination of single grain fusion and single grain stepped heating experiments on both K-feldspar and biotite crystals using a 50 W Synrad CO_2 laser. Gas clean-up was through an all-metal extraction line with a -130 °C cold trap, to remove H_2O, and two water-cooled SEAES GP-50 getters to absorb reactive gases. The Ar-isotope analyses were carried out on a Nu Instruments Noblesse multi-collector noble gas mass spectrometer. Analytical procedures, previously documented in Brumm et al., (2010) are detailed in the supplementary information file and all results, correction factors and constants are given in the supplementary data file. As previous studies on similar material (Wilson et al., 2007) had reported high levels of contamination with Cl, which can cause an isobaric interference with ^{36}Ar in the mass spectrometer by formation of $^{1}H^{35}Cl$, ^{35}Cl was measured in addition to the Ar-isotope analyses to monitor for Cl contamination, none of which was observed.

3. $^{40}Ar/^{39}Ar$ Results

Results of the Ar-isotope single crystal analyses are given in supplementary Tables 2 and Figures 4 - 7. K-feldspar single grain fusion ages (excluding data with blank-corrected ^{40}Ar yields of less than 0.5 mV (~30,000 cps) and zero $^{40}Ar^*$ yields; n = 27) range from 31 ± 5 ka to 125 ± 18 ka, indicating that some grains record pre-eruption model ages, i.e. they are either xenocrystic or contain excess ^{40}Ar. Biotite single grain fusion ages (n=4) range from 39 ± 8 ka to 57 ± 6 ka. An isotope correlation diagram plotting all of the single crystal fusion data (Figure 5) gives an inverse isochron age of 55.3 ± 1.8 ka.

Stepped heating experiments were carried out on 5 K-feldspar and 1 biotite crystals, yielding 3 steps for the K-feldspars and 4 steps for the biotite, although some of these steps produced exceptionally low ^{40}Ar, $^{40}Ar^*$ and / or ^{39}Ar gas yields. The individual step heating data yielded apparent ages from 39 ± 8 ka to 105 ± 16 ka.

Three of the five K-feldspar crystals gave high apparent ages for the first temperature step (up to 105 ka) and exhibit decreasing age with increasing temperature (e.g. 2608-02, Figure 4) while a fourth followed the same pattern but the first and final temperature steps yielded < 0.5 mV ^{40}Ar and so have been discounted. Isochrons could not be calculated for these crystals. Stepped heating of K-feldspar 2608-04 yielded

consistent ages for all three temperature steps, giving a 3-step "plateau" age of 50 ± 4 ka (Figure 4) and a 3-point isochron age of 51 ± 0.5 ka ($^{40}Ar/^{36}Ar$ = 298 ± 3, MSWD = 0.5, p = 0.48). Stepped heating was attempted on one biotite crystal using 4 temperature (laser power) steps. The first two of these steps released gas with an $^{40}Ar/^{36}Ar$ composition within uncertainty of the atmospheric ratio of 298.56, and can be attributed to the release of loosely adhering atmospheric argon from gentle heating of the crystal.

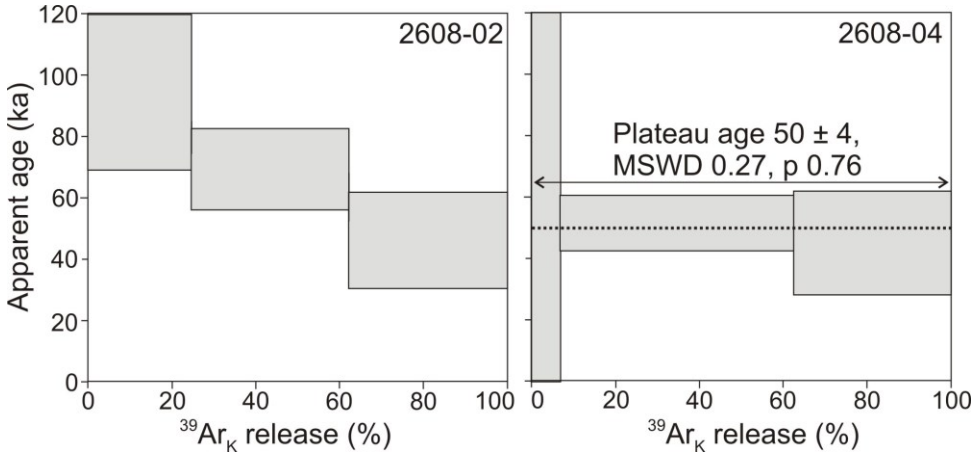

Figure 4. $^{40}Ar/^{39}Ar$ age spectra from stepped heating experiments on single K-feldspar crystals. Crystal 2608-02 shows a gas release pattern of decreasing model age with increasing temperature and suggests that excess ^{40}Ar is present in fluid and magmatic inclusions in the crystals. By contrast, crystal 2608-04 exhibits a flat release spectrum and younger age, suggesting that it is either unaffected by, or at least less influenced by excess ^{40}Ar. Error boxes on the spectra are 2σ and all quoted errors are 1σ.

$^{40}Ar/^{39}Ar$ ages from stepped heating of individual crystals that vary beyond normal analytical uncertainties can be interpreted in terms of excess ^{40}Ar, inherited ^{40}Ar in xenocrystic or antecrystic cores, or as ^{39}Ar loss due to recoil. These possibilities are discussed below.

4. Interpretation of variable model $^{40}Ar/^{39}Ar$ ages

4.1 Inherited $^{40}Ar^*$.

Inherited $^{40}Ar^*$ is a possible reason for older ages observed in both stepped heating and fusion analyses. The granitoid clasts are interpreted as having crystallised in multiple stages (Brown et al., 1998; Burt et al.,

1998) and contain zircons that record pre-eruption ages (Charlier et al., 2003) and so it would be expected that these clasts contain antecrystic material. However, we purposefully selected crystals lining miarolytic cavities in the clasts to avoid antecrysts retaining $^{40}Ar^*$ older than the eruption. The bulk of sample 103/1 has a sugary, friable texture, indicative of gas exsolution and quenching of interstitial melt to form volcanic glass. The glass was considered by Brown et al., (1998) to be interstitial melt, rather than infiltrated melt or partial melt during reheating based on textural and chemical analysis. The presence of glass quenched from interstitial melt indicates that the granitoid remained partially molten until eruption and will have sustained elevated temperatures; Brown et al., (1998) suggested a feldspar thermometry crystallisation temperature of 700 °C for the later stage, supercooled crystals. Granophyric texture (Figure 3) and miarolytic cavities are further evidence that this sample crystallised and quenched during transport to the surface (Brown et al., 1998; Burt et al., 1998) and it is difficult to envisage a scenario where miarolytic cavities and glass could form in the subsurface and be retained over geochronologically significant timescales without being modified.

If the crystals we analysed did form thousands of years before the eruption and retained a portion of their $^{40}Ar^*$, we would expect this to be reflected in the age spectra produced by stepped heating experiments. Inherited $^{40}Ar^*$ would diffuse out of the crystal while ever the crystal is held at elevated temperature in the subsurface and / or during eruption and so the highest concentration of $^{40}Ar^*$ would be in the core of the crystal. This would manifest on age spectra as younger ages in the early steps and older ages in the latter steps. This pattern is opposite to what is observed for stepped heating of single feldspar crystals, which produce the oldest ages in the earliest steps.

As a further check, we carried out diffusion modelling to assess whether a feldspar that crystallised as part of a partially molten mush, thousands of years before the eruption, would retain any $^{40}Ar^*$ and thus give older ages. We considered a simplified scenario where an Ar-bearing feldspar was held at 700 °C and modelled the fractional Ar loss experienced by the crystal. We assumed a spherical crystal of radius of 0.5 mm (the largest crystals analysed), $D_0 = 0.0098$ cm^2 s^{-1} and E = 44 kcal mol^{-1} (Foland, 1994) and used the fractional loss equations given in McDougall and Harrison (1999). Under these conditions, 100% of the Ar in

the crystal would have been lost after just 40 years. Feldspars of this size that crystallised thousands of years before the eruption would only retain a significant proportion (>50%) of their $^{40}Ar^*$ at temperatures < 500 °C; the evidence for interstitial melt in the granitoid clasts is not consistent with such low temperatures.

4.2 Recoil of ^{39}Ar

Recoil of ^{39}Ar during neutron irradiation may result in ejection of ^{39}Ar atoms from the crystal lattice and can be a problem for samples where the grain size is approaching the ^{39}Ar recoil distance (partial depletion layer thickness of 0.7 µm - (Jourdan et al., 2007)). Recoil typically manifests on age spectra as a stepwise decrease in age with increasing temperature, similar to that observed during stepped heating of our individual feldspar crystals; gas release from early temperature steps is dominated by that from the smaller grain sizes most affected by recoil and the relative depletion in ^{39}Ar relative to $^{40}Ar^*$ results of over-estimation of the $^{40}Ar/^{39}Ar$ age.

In the case of our Rotoiti samples, individual crystals are ~ 1mm diameter or larger; many appear fractured in thin section (Fig. 3B) but these fracture domains are still tens of microns in diameter and thus unlikely to be affected by recoil. It is possible that the observed patches of streaky extinction and very fine lamellae in some of the K-feldspar crystals represent structures that could facilitate recoil of ^{39}Ar, but these often occur as discrete patches interspersed with areas that are more homogenous and it is likely that such a scenario would not produce the “classic” decreasing age spectrum associated with recoil.

4.3 Excess ^{40}Ar

Excess ^{40}Ar hosted in melt or fluid inclusions may produce age spectra with older apparent ages in the early temperature steps; decrepitation of the inclusions releases the excess ^{40}Ar during the earliest heating stages and contributes to the classic “saddle-shaped” age spectrum associated with excess ^{40}Ar.

The age spectra produced by stepped heating of individual crystals (Fig. 4) are consistent with fluid / magmatic inclusion-hosted excess ^{40}Ar. Futhermore, many K-feldspars in sample 103/1, contain an abundance of magmatic and / or fluid inclusions (Figure 3).

The stepped heating data suggest that this excess ^{40}Ar is present in varying degrees in many, but not all of the crystals; the flat release and younger apparent age of crystal 2608-04 suggests that it contains little or no excess ^{40}Ar. If excess ^{40}Ar is inhomogeneously distributed within a sample (e.g. in clusters of fluid or magmatic inclusions, as observed in the photomicrographs in Figure 3), especially if it is decoupled from an atmospheric component (i.e. 3-way mixing between radiogenic, atmospheric and excess Ar), it can be difficult or impossible to identify using isotope correlation diagrams as regressions of the data will tend to yield an atmospheric intercept and an apparent age that is too old (Kuiper, 2002).

4.4 Eruption age vs. excess ^{40}Ar age

Plotting the stepped heating data from all six (5 K-feldspar, 1 biotite) crystals onto an isotope correlation diagram produces an apparent age of 54 ± 3 ka with a trapped ^{40}Ar/^{36}Ar content of 298.9 ± 1.6 (n=14/16, two data points automatically rejected by the Mass Spec software). In Figure 5 the data are plotted according to their temperature step; low temperature steps (light grey) tend to lie below the isochron line while the higher temperature steps (black) lie on or above the line. The isochron has an atmospheric intercept, despite an excess ^{40}Ar component clearly being identified on age spectra. Such a distribution of data points is consistent with a scenario involving mixing of atmospheric, radiogenic and excess ^{40}Ar, as described by (Kuiper, 2002). Data points not affected by excess ^{40}Ar would define an isochron formed by a mixing line between radiogenic and atmospheric end-members, with an atmospheric intercept. Heterogeneous incorporation of excess ^{40}Ar, as a source of trapped Ar additional to atmosphere, shifts the data points downwards and to the left of the isochron line. This has the net effect of increasing the slope of the calculated isochron line, resulting in an older age, whilst maintaining an atmospheric intercept; such an apparent isochron is an artefact and does not represent mixing between a single trapped and radiogenic end members (Kuiper, 2002). The high MSWD (2) suggests that the scatter of the data is greater than would be expected based on the errors on the individual data points and this is consistent with this interpretation

of variably-distributed excess ^{40}Ar. Inspection of the stepped heating isochron shows that it is dominated by data from the middle and high temperature steps. Given that the middle temperature steps may still contain excess ^{40}Ar, this isochron age is considered to be an over-estimate and an upper limit of the eruption age.

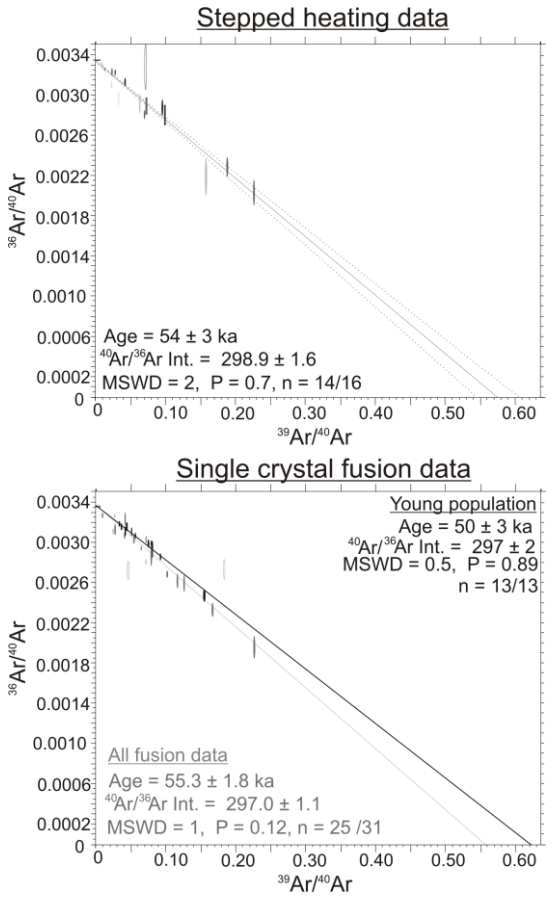

Figure 5: Isotope correlation diagrams created using the software Mass Spec (Al Deino, Berkeley Geochronology Center). Isochron ages were calculated invoking an automated data filtering process to eliminate outliers on the basis of their large contribution to the weighted sum of squares of the linear regression of the data. Top panel: Isotope correlation diagram combining stepped heating data from 6 individual crystal stepped heating experiments: 5 K-feldspar (ellipses) and 1 biotite (squares). The first two biotite temperature steps were dominated by air and have been excluded from the diagrams for clarity. Light grey symbols = low temperature steps (~0.5W), dark grey symbols = medium temperature steps (~1.5 W) and black symbols = high temperature steps (4-10 W). Bottom panel: Isotope correlation diagram of the single crystal fusion data. Ellipses = K-felsdpar data, squares = biotite data. Filled symbols show the data contributing to the grey isochron line (55.3 ± 1.1 ka) which is based on all of the single crystal fusion data. Black symbols represent the data points thought to be least-contaminated by excess ^{40}Ar (see main text on the unmixing model) and form an isochron with an age of 50 ± 3 ka.

309 Next we consider whether the single crystal total fusion data can improve our estimate of the eruption age.
310 If we assume that each crystal contains a different amount of excess ^{40}Ar, and that some crystals contain
311 little or no excess ^{40}Ar as shown by the step-heating experiments, we can treat the dataset as a mixture of
312 populations with different apparent ages, and that the youngest coherent age population represents the
313 crystals least contaminated with excess ^{40}Ar and is a best-estimate of the eruption age.

314 To identify the youngest coherent age population, ages were initially analysed using the Isoplot unmixing
315 tool (Ludwig, 2008), which is based on Sambridge and Compston's (1994) algorithms for deconvoluting
316 mixtures of similar age zircon populations. These algorithms aim to determine the true number of age
317 components, their age values, and their relative proportions using an iterative procedure; the exact values
318 of the true age and relative proportions of the different populations are not directly recoverable and,
319 instead, the model makes a best estimate of the ages and proportions, based on a maximised likelihood of
320 the data representing multiple age components (Sambridge and Compston, 1994). The procedure begins
321 with a guess of the number of age components (age populations) and returns an estimate of the ages (with
322 error), relative proportions of those components and likelihood that the data are best described by those
323 components (the likelihood is returned as the inverse log of the likelihood – the relative misfit parameter).
324 The procedure is repeated using a different number of components until a minimum value for the relative
325 misfit parameter is achieved. The model assumes that all populations have a Gaussian distribution. The
326 relative proportions are calculated as the ratio of the areas beneath each population's distribution curve
327 (Figure 6) (Sambridge and Compston, 1994).

328 Use of this model to fully assess our single crystal fusion data is a little problematic because of the
329 requirement for a Gaussian age distribution; while we expect the analyses not contaminated with excess
330 ^{40}Ar to approximate a Gaussian distribution, this is unlikely for the variable contaminated crystals and the
331 actual spread of ages in this population is likely to include a substantial tail to older ages. To maximise the
332 likelihood of the model giving meaningful results, we attempted to remove the non-Gaussian tail from the
333 excess ^{40}Ar contaminated population by excluding all ages greater than Wilson et al's (1992) initial age
334 estimate of 64 ka. We also excluded the three youngest data (all of which gave geologically unreasonable

ages of <32 ka). For the remaining 22 data points, a minimum value for the relative misfit parameter (1.044) was achieved by invoking 2 populations with the youngest population estimated at 47.9 ± 2.1 ka and formed by 55% of the data and the older population estimated at 56.9 ± 3.6 ka and formed by 45% of the data (Figure 6).

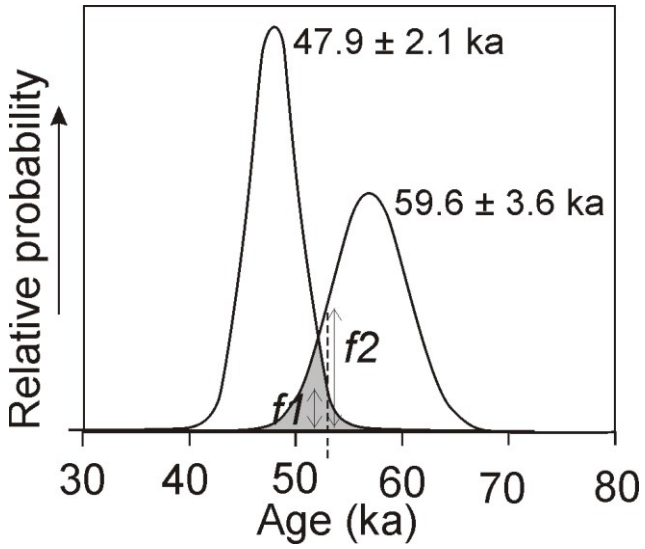

Figure 6: Sambridge and Compston's (1994) unmixing model for the single crystal fusion $^{40}Ar/^{39}Ar$ age data. Using Isoplot, the unmixing model suggests two populations are present: a younger population (estimated age 47.9 ± 2.1 ka, 55%) and an older, excess ^{40}Ar contaminated population (estimated age 59.6± 3.6 ka, 45%). The relative proportions of the populations are calculated by ratioing the area beneath the population curves. Where the curves overlap (grey shading), it is difficult to conclusively assign individual data points to each population. The diagram shows a hypothetical analysis with an age of 53 ka (dashed line) - the probability of this analysis belonging to the older population (f2) is greater than the probability of it belonging to the younger population (f1), but it could belong to either.

This unmixing model was used to select analyses belonging to the youngest population from which to calculate a weighted average. Assigning each individual analysis to a population becomes difficult for ages that are described by both populations (shaded area on Figure 6). All ages > 52 ka (the point where the two population distribution curves cross) have a higher probability of belonging to the older population than the younger population (see case study of a hypothetical 53 ka data point in Figure 6). Simply assuming that the youngest 55% of the data (i.e. the youngest 12 analyses) represent the youngest population is likely to exclude data that do belong to the younger population, but have ages > 52 ka. Instead we consider the range of ages beneath the young population distribution curve as a guide to selecting data that are not

contaminated by excess ^{40}Ar and use 55 ka as an upper limit for data belonging to the young population. Using this criterion, 13 out of the 22 analyses were assigned to the young population (39 ± 8 to 52 ± 4 ka). A weighted average of these data gives an age of 47.4 ± 1.5 ka with a statistically acceptable MSWD (according to the criteria of Wendt and Carl, 1991) of 0.58 for n = 13 and a probability of fit of 0.86. Figure 7 shows this weighted average in the context of the individual data, the distribution curves for the population unmixing model, and our cut-off point for selecting data representative of the young population.

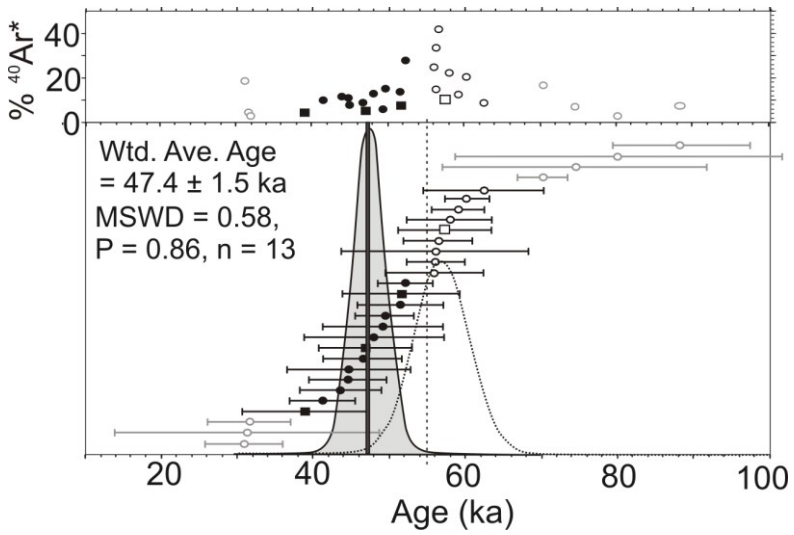

Figure 7: Single crystal fusion ages (circles = K-feldspar, squares = biotite) shown with the age distribution of the two populations identified by the unmixing model (curves) and the 55 ka cut-off for selecting analyses belonging to the youngest population (dashed vertical line). Grey symbols are data excluded from the unmixing analyses to allow an approximation of Gaussian distribution for the populations. Filled symbols represent data assigned to the young population. Open symbols represent data contaminated with excess ^{40}Ar and thus yield ages older than the eruption. Circles = K-feldspar, squares = biotite. Black vertical line is the weighted average ± 1σ of the young population (n=13). Error bars on individual analyses are 1 σ.

A further assessment of this age was carried out by plotting an isochron of the data assigned to the young population, giving an age of 50 ± 3 ka, a $^{40}Ar/^{36}Ar$ intercept of 297 ± 2, and an MSWD of 0.5. Figure 5 (lower panel) compares this isochron to the full single crystal fusion data set. This isochron age is indistinguishable from both the weighted average age and the youngest population derived by the unmixing model. Visual inspection of the single crystal fusion isochron plots in Figure 5 shows that the data thought to belong to

the young population form a trend that is qualitatively different from the other analyses, as would be expected when comparing an excess ^{40}Ar-free population with data that are contaminated with excess ^{40}Ar.

5. Discussion and implications

Our preferred estimate of the eruption age is the statistically robust weighted mean (47.4 ± 1.5 ka). It is consistent with a number of previously published ages for the Rotoiti eruption (Berryman, 1993, 1993; Buhay et al., 1992; Charlier et al., 2003; Danišík et al., 2012; Lian and Shane, 2000; Molloy et al., 2009; Nilsson et al., 2011; Santos et al., 2001; Shane et al., 2006; Shane and Sandiford, 2003), but is significantly younger than Wilson et al.'s (2007) age. The latter (61.0 ± 1.4 ka) is based on extrapolation between a K-Ar age for an underlying lava flow and a ^{40}Ar/^{39}Ar age for an overlying obsidian lava flow (58.5 ± 1.1 ka) that bracket the Rotoehu ash on Mayor Island. Regardless of accuracy of Wilson et al's age extrapolation to the Rotoehu ash, the ^{40}Ar/^{39}Ar age of the overlying lava flow should be younger than that of the Rotoiti eruption; this is not observed for our new eruption age and this discrepancy warrants discussion.

In addition to the overlying lava age, Wilson et al (2007) also report ^{40}Ar/^{39}Ar ages from stepped heating experiments carried out on multi-grain aliquots of biotite and plagioclase separated from the Rotoiti Pumice, fused lithic clasts similar to the sample analysed in this study, and from the Earthquake Flat Pumice. While some of these ages clearly reflect contamination with excess or inherited ^{40}Ar, others are comparable to Wilson et al's proposed eruption age. However, almost half of these ages overlap with our proposed eruption age at 2 standard deviations. Furthermore, as previously noted by Danišík et al. (2012), Wilson et al state that initial stepped heating experiments on biotites from fused lithics yielded younger isochron ages of 47 and 55 ka, but that these were discarded as they were at odds with the bracketing lava ages.

It seems the main discrepancy between our proposed age and that of Wilson et al (2007) concerns the ages of the overlying Mayor Island lava, which was determined on obsidian from the basal carapace. Either this obsidian age is too old or our K-feldspar and biotite ages are too young. To investigate if the discrepancy between our Rotoiti eruption age and Wilson et al's (2007) overlying lava flow age can be explained by

differences in assumed fluence monitor age, we recalculated both Mayor Island and Rotoiti eruption ages according to different monitor ages.

Wilson et al (2007) used Taylor Creek sanidine (TCs) as their neutron fluence, with an assumed age of 27.87 Ma (Calvert and Lanphere, 2006), while we used ACs with an age of 1.1851 Ma (Rivera et al., 2013). Published ages for TCs range from 27.87 – 28.62 ka (Duffield and Dalrymple, 1990; Karner and Renne, 1998; Kuiper et al., 2008; Renne et al., 2010; Sarna-Wojcicki et al., 2000), while recent published ACs ages range from 1.180 ± 0.0025Ma (Coble et al., 2011) to 1.2056 ± 0.0019 Ma (Renne et al., 2011). Recalculating the Mayor Island obsidian flow using a TCs age of 28.62 Ma increases the obsidian age from 58.5 ka to 60.1 ka. Recalculating our 47.4 ka Rotoiti eruption age using ACs ages of 1.180 Ma and 1.2056 Ma gives ages of 47.2 ka and 48.2 ka respectively. Our eruption age remains significantly younger than Wilson et al's age for the overlying lava and this discrepancy cannot be explained by differences in fluence monitor age.

Young apparent $^{40}Ar/^{39}Ar$ ages may result from loss of $^{40}Ar^*$ during reheating or alteration or by over-correction for atmospheric ^{40}Ar by an apparent excess of ^{36}Ar. Loss of radiogenic $^{40}Ar^*$ during reheating is not thought to be an issue for our samples as these volcanic rocks have remained at the surface of the earth since they were erupted and so have not experienced subsequent heating events. While alteration may be an issue for a minority of analyses, our K-feldspar crystals were fresh with a glassy appearance and were often optically clear and euhedral while the biotite crystals appeared fresh and unaltered. Apparent excesses of ^{36}Ar may occur due to isobaric interferences in the mass spectrometer from ($^{12}C_3$) and ($^{1}H^{35}Cl$). We do not think this is likely as the Noblesse is able to partially resolve ^{36}Ar from ($^{12}C_3$) and mass 35 was measured for each analysis to monitor Cl contamination, but never yielded analyses greater than blank values. If a fractionated Ar-isotope component enriched in ^{36}Ar were incorporated homogenously into the crystals, this would result in younger individual apparent ages, but not affect the isochron ages and be detectable on isotope correlation diagrams. Inhomogeneous incorporation of excess ^{36}Ar may not be detectable, but this fractionated component would also have to reside in the crystal lattice and be released at high-temperatures to reproduce the stepped heating data, which seems unlikely. Furthermore, excess ^{36}Ar has not been documented in crystalline materials before.

Whilst obsidian has been successfully used to produce geologically meaningful $^{40}Ar/^{39}Ar$ ages (Flude et al., 2010; Morgan et al., 2009; Vogel et al., 2006), it is known to be problematic for reasons that are only just starting to become clear, and it is at least qualitatively possible that these poorly-understood processes can result in over-estimation of $^{40}Ar/^{39}Ar$ age spectra and isochron ages. Brown et al. (2009) and Morgan et al. (2009) suggested that the Ar-isotope composition of obsidians in Ethiopia had been affected by kinetic isotope fractionation of atmospheric gas either prior to or during absorption, while Flude et al. (in prep) concluded that kinetic isotope fractionation during magmatic degassing produced heterogeneously distributed excess ^{40}Ar due to preferential loss of ^{36}Ar during degassing. As already discussed, when distributed heterogeneously, excess ^{40}Ar may be difficult to detect via age spectra and isotope correlation diagrams (Kuiper, 2002; Sherlock and Arnaud, 1999), and this may be exacerbated when step-heating aliquots of crushed obsidian which may mix small-scale isotope reservoirs and destroy any naturally occurring isotope profiles that might be detected by stepped-heating of a single fragment (i.e. the laboratory diffusion dimension is less than the natural diffusion dimension). Furthermore, if kinetic isotopic fractionation were to take place during stepped heating of obsidian in the laboratory we would expect ^{36}Ar to be released faster than ^{40}Ar, resulting in relative depression of $^{40}Ar/^{36}Ar$ values in the earliest heating steps and elevation in the later heating steps. Isochrons from such data may give apparent ages that are too high with $^{40}Ar/^{36}Ar$ intercepts that are too low, thus obscuring the presence of any excess ^{40}Ar and yielding an incorrect but seemingly robust apparent $^{40}Ar/^{39}Ar$ age.

We are unable to identify a mechanism that could result in our proposed eruption age being under-estimated by ~10-15 kyrs, but it is possible that Wilson et al's (2007) obsidian age is an over-estimate. We also note that our proposed eruption age is within error of many other age estimates for the Rotoiti eruption, is consistent with palaeoenvironmental interpretations (Shane and Sandiford, 2003), and that there are now three radio-isotope techniques (^{14}C, U-Th-He, $^{40}Ar/^{39}Ar$) that have yielded consistent eruption ages ~ 45-47 ka. As previously discussed by Danišík et al. (2012), adopting a younger age for the Rotoiti eruption suggests that the TVZ has been much more active than previously realised. Revision

453 increases silicic magma production rates for the Okataina caldera complex from 2.5 km^3 ka^{-1} (Wilson et al.,
454 1995) to 3.8 km^3 ka^{-1} and magma eruption rates of the TVZ are revised to~ 17 km^3 kyr^{-1}.

455 **5. Conclusions**

456 Vapour phase crystallisation of K-feldspar and biotite in miarolytic cavities of glass-bearing granitoid clasts
457 entrained in the eruption of the Rotoiti ignimbrite provide high-K phases suitable for $^{40}Ar/^{39}Ar$ dating of this
458 young, difficult to date eruption. Stepped-heating Ar-isotope analyses on single crystals indicate that excess
459 ^{40}Ar is present in fluid and / or magmatic inclusions present in some of the crystals and is released at low
460 temperatures. This excess ^{40}Ar component is variable and not present in every crystal and so isotope
461 correlation diagrams using single crystal fusion data represent mixing between three components of ^{40}Ar
462 (radiogenic, atmospheric and excess) and do not provide accurate trapped Ar compositions or $^{40}Ar/^{39}Ar$
463 ages. An isochron of the stepped heating data is dominated by the moderate-high temperature heating
464 steps and gives an upper limit of the eruption age of 54 ± 3 ka.

465 The eruption age can be further refined by treating the single-crystal fusion data as a mixed population and
466 assuming that the youngest cohesive age population represents the eruption age. A population unmixing
467 model was used to identify a young population, free from excess ^{40}Ar contamination. This population gave a
468 statistically valid weighted mean eruption age of 47.4 ± 1.5 ka which is indistinguishable from recent (U-
469 Th)/He and ^{14}C age determinations by Danišík et al. (2012) and from various other published age
470 determinations based on marine and lake sedimentation rates. However, our new age is significantly
471 younger than the $^{40}Ar/^{39}Ar$ age for an obsidian lava flow overlying the Rotoehu ash on Mayor Island,
472 presented by Wilson et al. (2007) and this discrepancy may be explained by kinetic fractionation of Ar-
473 isotopes in obsidian both in nature and the laboratory.

474 **Acknowledgements**

475 Fieldwork in New Zealand was carried out by MS during tenure of a 1-year fellowship at the University of
476 Waikato. The Quaternary Dating Laboratory at Roskilde University is funded by the Villum Foundation. This

manuscript benefitted from comments and discussion by reviewers Andy Calvert and an anonymous reviewer, and Editor Paul Renne.

References

Allan, A.S.R., Baker, J.A., Carter, L., Wysoczanksi, R.J., 2008. Reconstructing the Quaternary evolution of the world's most active silicic volcanic system: insights from an ~1.65 Ma deep ocean tephra record sourced from Taupo Volcanic Zone, New Zealand. Quaternary Science Reviews 27, 2341–2360. doi:10.1016/j.quascirev.2008.09.003

Berryman, K., 1992. A stratigraphic age of Rotoehu Ash and late Pleistocene climate interpretation based on marine terrace chronology, Mahia Peninsula, North Island, New Zealand. New Zealand Journal of Geology and Geophysics 35, 1–7. doi:10.1080/00288306.1992.9514494

Berryman, K.R., 1993. Distribution, age, and deformation of Late Pleistocene marine terraces at Mahia Peninsula, Hikurangi Subduction Margin, New Zealand. Tectonics 12, 1365–1379. doi:10.1029/93TC01543

Brown, F.H., Reid, C., Negash, A., 2009. Possible isotopic fractionation of argon in source obsidians and archeological artifacts from Kulkuletti, Ethiopia. Journal of Archaeological Science 36, 2119–2124. doi:10.1016/j.jas.2009.05.008

Brown, S.J.., Burt, R.., Cole, J.., Krippner, S.J.., Price, R.., Cartwright, I., 1998. Plutonic lithics in ignimbrites of Taupo Volcanic Zone, New Zealand; sources and conditions of crystallisation. Chemical Geology 148, 21–41. doi:10.1016/S0009-2541(98)00026-6

Brumm, A., Jensen, G.M., van den Bergh, G.D., Morwood, M.J., Kurniawan, I., Aziz, F., Storey, M., 2010. Hominins on Flores, Indonesia, by one million years ago. Nature 464, 748–752. doi:10.1038/nature08844

Buhay, W.M., Clifford, P.M., Schwarcz, H.P., 1992. ESR dating of the Rotoiti Breccia in the Taupo volcanic zone, New Zealand. Quaternary Science Reviews 11, 267–271. doi:10.1016/0277-3791(92)90072-G

Burt, R.M., Brown, S.J.A., Cole, J.W., Shelley, D., Waight, T.E., 1998. Glass-bearing plutonic fragments from ignimbrites of the Okataina caldera complex, Taupo Volcanic Zone, New Zealand: remnants of a partially molten intrusion associated with preceding eruptions. Journal of Volcanology and Geothermal Research 84, 209–237. doi:10.1016/S0377-0273(98)00039-0

Calvert, A.T., Lanphere, M.A., 2006. Argon geochronology of Kilauea's early submarine history. Journal of Volcanology and Geothermal Research 151, 1–18. doi:10.1016/j.jvolgeores.2005.07.023

Chappell, J., 2002. Sea level changes forced ice breakouts in the Last Glacial cycle: new results from coral terraces. Quaternary Science Reviews 21, 1229–1240. doi:10.1016/S0277-3791(01)00141-X

Chappell, J., Shackleton, N.J., 1986. Oxygen isotopes and sea level. Nature 324, 137–140. doi:10.1038/324137a0

Charlier, B.L.A., Wilson, C.J.N., 2010. Chronology and Evolution of Caldera-forming and Post-caldera Magma Systems at Okataina Volcano, New Zealand from Zircon U-Th Model-age Spectra. Journal of Petrology 51, 1121–1141. doi:10.1093/petrology/egq015

Charlier, B.L.., Peate, D.W., Wilson, C.J.., Lowenstern, J.B., Storey, M., Brown, S.J.., 2003. Crystallisation ages in coeval silicic magma bodies: 238U–230Th disequilibrium evidence from the Rotoiti and Earthquake Flat eruption deposits, Taupo Volcanic Zone, New Zealand. Earth and Planetary Science Letters 206, 441–457. doi:10.1016/S0012-821X(02)01109-3

Coble, M.A., Grove, M., Calvert, A.T., 2011. Calibration of Nu-Instruments Noblesse multicollector mass spectrometers for argon isotopic measurements using a newly developed reference gas. Chemical Geology 290, 75–87. doi:10.1016/j.chemgeo.2011.09.003

Danišík, M., Shane, P., Schmitt, A.K., Hogg, A., Santos, G.M., Storm, S., Evans, N.J., Keith Fifield, L., Lindsay, J.M., 2012. Re-anchoring the late Pleistocene tephrochronology of New Zealand based on concordant radiocarbon ages and combined 238U/230Th disequilibrium and (U–Th)/He zircon ages. Earth and Planetary Science Letters 349-350, 240–250. doi:10.1016/j.epsl.2012.06.041

Duffield, W., Dalrymple, Gb., 1990. The Taylor Creek Rhyolite of New Mexico: a rapidly emplaced field of lava domes and flows. Bull Volcanol 52, 475–487. doi:10.1007/BF00268927

527 Ewart, A., Cole, J.W., 1967. Textural and mineralogical significance of the Granitic Xenoliths from the
528 Central Volcanic Region, North Island, New Zealand. New Zealand Journal of Geology and
529 Geophysics 10, 31–54. doi:10.1080/00288306.1967.10428183
530 Flude, S., McGarvie, D.W., Burgess, R., Tindle, A.G., 2010. Rhyolites at Kerlingarfjöll, Iceland: the evolution
531 and lifespan of silicic central volcanoes. Bulletin of Volcanology 72, 523–538. doi:10.1007/s00445-
532 010-0344-0
533 Flude, S., Tuffen, H., Sherlock, S.C., Kelley, S.P., in prep. Excess 40Ar in obsidian from Ar-isotope
534 fractionation during magmatic degassing.
535 Foland, K.A., 1994. Argon diffusion in feldspars, in: Parsons, I. (Ed.), Feldspars and Their Reactions. Kluwer
536 Academic Publishers.
537 Froggatt, P.C., Lowe, D.J., 1990. A review of late Quaternary silicic and some other tephra formations from
538 New Zealand: Their stratigraphy, nomenclature, distribution, volume, and age. New Zealand
539 Journal of Geology and Geophysics 33, 89–109. doi:10.1080/00288306.1990.10427576
540 Grant-Taylor, T.L., Rafter, T.A., 1971. New Zealand radiocarbon age measurements — 6. New Zealand
541 Journal of Geology and Geophysics 14, 364–402. doi:10.1080/00288306.1971.10421932
542 Jourdan, F., Matzel, J.P., Renne, P.R., 2007. 39Ar and 37Ar recoil loss during neutron irradiation of sanidine
543 and plagioclase. Geochimica et Cosmochimica Acta 71, 2791–2808. doi:10.1016/j.gca.2007.03.017
544 Karner, D.B., Renne, P.R., 1998. 40Ar/39Ar geochronology of Roman volcanic province tephra in the Tiber
545 River valley: Age calibration of middle Pleistocene sea-level changes. Geological Society of America
546 Bulletin 110, 740–747. doi:10.1130/0016-7606(1998)110<0740:AAGORV>2.3.CO;2
547 Kimber, R.W.L., Kennedy, N.M., Milnes, A.R., 1994. Amino acid racemization dating of a 140 000 year old
548 tephra-loess-palaeosol sequence on the Mamaku Plateau near Rotorua, New Zealand. Australian
549 Journal of Earth Sciences 41, 19–26. doi:10.1080/08120099408728109
550 Kuiper, K.F., Deino, A., Hilgen, F.J., Krijgsman, W., Renne, P.R., Wijbrans, J.R., 2008. Synchronizing Rock
551 Clocks of Earth History. Science 320, 500–504. doi:10.1126/science.1154339
552 Kuiper, Y.D., 2002. The interpretation of inverse isochron diagrams in 40Ar/39Ar geochronology. Earth and
553 Planetary Science Letters 203, 499–506. doi:10.1016/S0012-821X(02)00833-6
554 Lian, O.B., Shane, P.A., 2000. Optical dating of paleosols bracketing the widespread Rotoehu tephra, North
555 Island, New Zealand. Quaternary Science Reviews 19, 1649–1662. doi:10.1016/S0277-
556 3791(00)00003-2
557 Lofgren, G.E., Gooley, R., 1977. Simultaneous crystallization of feldspar intergrowths from the melt.
558 American Mineralogist 62, 217–228.
559 Lowe, D.J., Hogg, A.G., 1995. Letter to the Editor: Age of the Rotoehu Ash Comment. New Zealand Journal
560 of Geology and Geophysics 38, 399–402. doi:10.1080/00288306.1995.9514666
561 Ludwig, K.R., 2008. User's manual for Isoplot 3.7: A geochronological Toolkit for Microsoft Excel.
562 McDougall, I., Harrison, T.M., 1999. Geochronology and Thermochronology by the 40Ar/39Ar method, 2nd
563 Edition. ed. Oxford University Press.
564 Mcglone, M.S., Howorth, R., Pullar, W.A., 1984. Late Pleistocene stratigraphy, vegetation and climate of the
565 Bay of Plenty and Gisborne regions, New Zealand. New Zealand Journal of Geology and Geophysics
566 27, 327–350.
567 Molloy, C., Shane, P., Augustinus, P., 2009. Eruption recurrence rates in a basaltic volcanic field based on
568 tephra layers in maar sediments: Implications for hazards in the Auckland volcanic field. Geological
569 Society of America Bulletin 121, 1666–1677. doi:10.1130/B26447.1
570 Molloy, C., Shane, P., Nairn, I., 2008. Pre-eruption thermal rejuvenation and stirring of a partly crystalline
571 rhyolite pluton revealed by the Earthquake Flat Pyroclastics deposits, New Zealand. Journal of the
572 Geological Society 165, 435–447. doi:10.1144/0016-76492007-071
573 Morgan, L.E., Renne, P.R., Taylor, R.E., WoldeGabriel, G., 2009. Archaeological age constraints from
574 extrusion ages of obsidian: Examples from the Middle Awash, Ethiopia. Quaternary Geochronology
575 4, 193–203. doi:10.1016/j.quageo.2009.01.001
576 Nairn, I.A., Kohn, B.P., 1973. Relation of the Earthquake Flat Breccia to the Rotoiti Breccia, Central North
577 Island, New Zealand. New Zealand Journal of Geology and Geophysics 16, 269–279.
578 doi:10.1080/00288306.1973.10431457

Nathan, S., 1976. Age of the Rotoiti Breccia formation. Geological Society of New Zealand newsletter 41, 21–24.
Nilsson, A., Muscheler, R., Snowball, I., Aldahan, A., Possnert, G., Augustinus, P., Atkin, D., Stephens, T., 2011. Multi-proxy identification of the Laschamp geomagnetic field excursion in Lake Pupuke, New Zealand. Earth and Planetary Science Letters 311, 155–164. doi:10.1016/j.epsl.2011.08.050
Ota, Y., Omura, A., Iwata, H., 1989. ^{230}Th-^{238}U age of Rotoehu Ash and its implications for marine terrace chronology of eastern Bay of Plenty, New Zealand. New Zealand Journal of Geology and Geophysics 32, 327–331. doi:10.1080/00288306.1989.10425712
Pillans, B., Wright, I., 1992. Late Quaternary tephrostratigraphy from the southern Havre Trough - Bay of Plenty, northeast New Zealand. New Zealand Journal of Geology and Geophysics 35, 129–143. doi:10.1080/00288306.1992.9514507
Pullar, W.A., 1976. Age of Rotoiti Breccia Formation. Geological Society of New Zealand newsletter 41, 22–23.
Pullar, W.A., Heine, J.C., 1971. Ages, inferred from 14C dates, of some tephra and other deposits from Rotorua, Taupo, Bay of Plenty and Hawke's Bay districts. Proceedings of Radiocarbon User's Conference, Lower Hitt 118–138.
Pullar, W.A., Nairn, I.A., 1972. Matahi Basaltic Tephra member, Rotoiti Breccia Formation. New Zealand Journal of Geology and Geophysics 15, 446–450. doi:10.1080/00288306.1972.10422342
Renne, P.R., Balco, G., Ludwig, K.R., Mundil, R., Min, K., 2011. Response to the comment by W.H. Schwarz et al. on "Joint determination of 40K decay constants and 40Ar∗/40K for the Fish Canyon sanidine standard, and improved accuracy for 40Ar/39Ar geochronology" by P.R. Renne et al. (2010). Geochimica et Cosmochimica Acta 75, 5097–5100. doi:10.1016/j.gca.2011.06.021
Renne, P.R., Mundil, R., Balco, G., Min, K., Ludwig, K.R., 2010. Joint determination of 40K decay constants and 40Ar∗/40K for the Fish Canyon sanidine standard, and improved accuracy for 40Ar/39Ar geochronology. Geochimica et Cosmochimica Acta 74, 5349–5367. doi:10.1016/j.gca.2010.06.017
Rivera, T.A., Storey, M., Schmitz, M.D., Crowley, J.L., 2013. Age intercalibration of 40Ar/39Ar sanidine and chemically distinct U/Pb zircon populations from the Alder Creek Rhyolite Quaternary geochronology standard. Chemical Geology 345, 87–98. doi:10.1016/j.chemgeo.2013.02.021
Sambridge, M.S., Compston, W., 1994. Mixture modeling of multi-component data sets with application to ion-probe zircon ages. Earth and Planetary Science Letters 128, 373–390. doi:10.1016/0012-821X(94)90157-0
Santos, G.M., Bird, M.I., Fifield, L.K., Alloway, B.V., Chappell, J., Hausladen, P.A., Arneth, A., 2001. Radiocarbon dating of wood using different pretreatment procedures; application to the chronology of Rotoehu Ash, New Zealand. Radiocarbon 43, 239–248.
Sarna-Wojcicki, A.M., Pringle, M.S., Wijbrans, J., 2000. New ^{40}Ar/^{39}Ar age of the Bishop Tuff from multiple sites and sediment rate calibration for the Matuyama-Brunhes boundary. Journal of Geophysical Research 105, 21431. doi:10.1029/2000JB900901
Shane, P., 2000. Tephrochronology: a New Zealand case study. Earth-Science Reviews 49, 223–259. doi:10.1016/S0012-8252(99)00058-6
Shane, P., Nairn, I.A., Smith, V.C., 2005. Magma mingling in the ~50 ka Rotoiti eruption from Okataina Volcanic Centre: implications for geochemical diversity and chronology of large volume rhyolites. Journal of Volcanology and Geothermal Research 139, 295–313. doi:10.1016/j.jvolgeores.2004.08.012
Shane, P., Sandiford, A., 2003. Paleovegetation of marine isotope stages 4 and 3 in northern new zealand and the age of the widespread rotoehu tephra. Quaternary Research 59, 420–429. doi:10.1016/S0033-5894(03)00044-9
Shane, P., Sikes, E.L., Guilderson, T.P., 2006. Tephra beds in deep-sea cores off northern New Zealand: implications for the history of Taupo Volcanic Zone, Mayor Island and White Island volcanoes. Journal of Volcanology and Geothermal Research 154, 276–290. doi:10.1016/j.jvolgeores.2006.03.021
Shane, P., Storm, S., Schmitt, A.K., Lindsay, J.M., 2012. Timing and conditions of formation of granitoid clasts erupted in recent pyroclastic deposits from Tarawera Volcano (New Zealand). Lithos 140–141, 1–10. doi:10.1016/j.lithos.2012.01.012

Sherlock, S.C., Arnaud, N.O., 1999. Flat plateau and impossible isochrons: apparent 40Ar-39Ar geochronology in a high-pressure terrain. Geochimica et Cosmochimica Acta 63, 2835–2838. doi:10.1016/S0016-7037(99)00116-7

Smith, V., Shane, P., Nairn, I., 2010. Insights into silicic melt generation using plagioclase, quartz and melt inclusions from the caldera-forming Rotoiti eruption, Taupo volcanic zone, New Zealand. Contrib Mineral Petrol 160, 951–971. doi:10.1007/s00410-010-0516-0

Thompson, B.N., 1968a. Notes from the New Zealand Geological Survey—5: Age of Rotoiti Breccia. New Zealand Journal of Geology and Geophysics 11, 1189–1191. doi:10.1080/00288306.1968.10420248

Thompson, B.N., 1968b. Notes from the New Zealand Geological Survey—5: Age of Rotoiti Breccia. New Zealand Journal of Geology and Geophysics 11, 1189–1191. doi:10.1080/00288306.1968.10420248

Vogel, N., Nomade, S., Negash, A., Renne, P.R., 2006. Forensic 40Ar/39Ar dating: a provenance study of Middle Stone Age obsidian artifacts from Ethiopia. Journal of Archaeological Science 33, 1749–1765. doi:10.1016/j.jas.2006.03.008

Vucetich, C.G., Pullar, W.A., 1969. Stratigraphy and chronology of late pleistocene volcanic ash beds in Central North Island, New Zealand. New Zealand Journal of Geology and Geophysics 12, 784–837. doi:10.1080/00288306.1969.10431112

Wendt, I., Carl, C., 1991. The statistical distribution of the mean squared weighted deviation. Chemical Geology: Isotope Geoscience section 86, 275–285. doi:10.1016/0168-9622(91)90010-T

Whitehead, N., Ditchburn, R., 1994. Revision of some ages for the Rotoehu Ash. New Zealand Journal of Geology and Geophysics 37, 381–383. doi:10.1080/00288306.1994.9514627

Wilson, C.J.N., Houghton, B.F., Lanphere, M.A., Weaver, S.D., 1992. A new radiometric age estimate for the Rotoehu Ash from Mayor Island volcano, New Zealand. New Zealand Journal of Geology and Geophysics 35, 371–374. doi:10.1080/00288306.1992.9514530

Wilson, C.J.N., Houghton, B.F., McWilliams, M.O., Lanphere, M.A., Weaver, S.D., Briggs, R.M., 1995. Volcanic and structural evolution of Taupo Volcanic Zone, New Zealand: a review. Journal of Volcanology and Geothermal Research 68, 1–28. doi:10.1016/0377-0273(95)00006-G

Wilson, C.J.N., Rhoades, D.A., Lanphere, M.A., Calvert, A.T., Houghton, B.F., Weaver, S.D., Cole, J.W., 2007. A multiple-approach radiometric age estimate for the Rotoiti and Earthquake Flat eruptions, New Zealand, with implications for the MIS 4/3 boundary. Quaternary Science Reviews 26, 1861–1870. doi:10.1016/j.quascirev.2007.04.017